JACS Au
AN OPEN ACCESS JOURNAL OF THE AMERICAN CHEMICAL SOCIETY

pubs.acs.org/jacsau

Article

C–H Bond Activation Mechanism by a Pd(II)–(μ-O)–Au(0) Structure Unique to Heterogeneous Catalysts

Daisuke Takei, Takafumi Yatabe,* Tomohiro Yabe, Ray Miyazaki, Jun-ya Hasegawa, and Kazuya Yamaguchi*

Cite This: JACS Au 2022, 2, 394–406

Read Online

ACCESS | Metrics & More | Article Recommendations | Supporting Information

ABSTRACT: We focused on identifying a catalytic active site structure at the atomic level and elucidating the mechanism at the elementary reaction level of liquid-phase organic reactions with a heterogeneous catalyst. In this study, we experimentally and computationally investigated efficient C–H bond activation for the selective aerobic α,β-dehydrogenation of saturated ketones by using a Pd–Au bimetallic nanoparticle catalyst supported on CeO_2 (Pd/Au/CeO_2) as a case study. Detailed characterization of the catalyst with various observation methods revealed that bimetallic nanoparticles formed on the CeO_2 support with an average size of about 2.5 nm and comprised a Au nanoparticle core and PdO nanospecies dispersed on the core. The formation mechanism of the nanoparticles was clarified through using several CeO_2-supported controlled catalysts. Activity tests and detailed characterizations demonstrated that the dehydrogenation activity increased with the coordination numbers of Pd–O species in the presence of Au(0) species. Such experimental evidence suggests that a Pd(II)–(μ-O)–Au(0) structure is the true active site for this reaction. Based on density functional theory calculations using a suitable $Pd_1O_2Au_{12}$ cluster model with the Pd(II)–(μ-O)–Au(0) structure, we propose a C–H bond activation mechanism via concerted catalysis in which the Pd atom acts as a Lewis acid and the adjacent μ-oxo species acts as a Brønsted base simultaneously. The calculated results reproduced the experimental results for the selective formation of 2-cyclohexen-1-one from cyclohexanone without forming phenol, the regioselectivity of the reaction, the turnover-limiting step, and the activation energy.

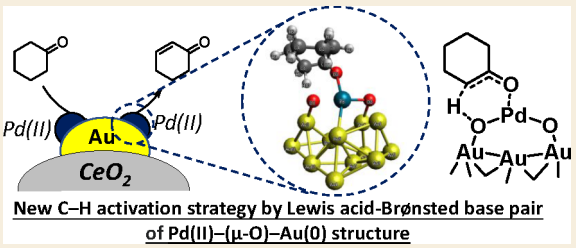

New C–H activation strategy by Lewis acid-Brønsted base pair of Pd(II)–(μ-O)–Au(0) structure

KEYWORDS: *C–H bond activation, heterogeneous catalysis, DFT study, Pd(II)–(μ-O)–Au(0) structure, aerobic dehydrogenation*

INTRODUCTION

C–H bond activation enables direct molecular transformations with excellent atomic efficiency in liquid-phase organic synthesis. Elucidating the mechanism of catalytic C–H bond activation is important for realizing environmentally friendly efficient molecular transformations.[1−6] Various mechanisms for C–H bond activation have been reported, such as oxidative addition,[7,8] concerted metalation-deprotonation (CMD),[9−11] and sigma-bond metathesis.[12−14] Most of the reported C–H bond activation systems for liquid-phase organic synthesis use homogeneous organometallic catalysts based on components of complexes: central metals and ligands.

Supported metal nanoparticle catalysts are easy to separate and reuse, which is an attractive feature for green chemistry. In addition, supported metal nanoparticle catalysts can create unique active site structures different from those of homogeneous complex catalysts and sometimes outperform homogeneous catalysts by utilizing their specific systems, such as the ensemble effect, ligand effect, concerted catalysis, and geometric structures (e.g., core–shell, cluster-in-cluster, and alloy structures).[15−19] Thus, supported metal nanoparticle catalysts have the potential to create novel active site structures for efficient C–H bond activation via unique mechanisms.[20] However, the reaction mechanism with supported metal nanoparticle catalysts and the structure of the catalytically active sites are not well understood at the elementary reaction level, which makes developing general heterogeneous catalyst design strategies extremely difficult.

Because the mechanism for molecular transformations by heterogeneous catalysts is still analogous and based on the understanding of homogeneous catalysts, theoretical approaches are necessary for elucidation. Many heterogeneous catalysts have been calculated through the use of cluster or slab models,[21−37] but most of these were focused on gas-phase reactions[21−26] such as CO oxidation.[21−23] Some liquid-phase fundamental organic reactions[27−37] have been evaluated such as alcohol oxidation,[27,28] coupling reactions,[29−33] and hydrogenation,[34,35] but other important elementary mechanisms in liquid-phase organic reactions including C–H bond activation

Received: October 1, 2021
Published: January 14, 2022

https://doi.org/10.1021/jacsau.1c00433
JACS Au 2022, 2, 394–406

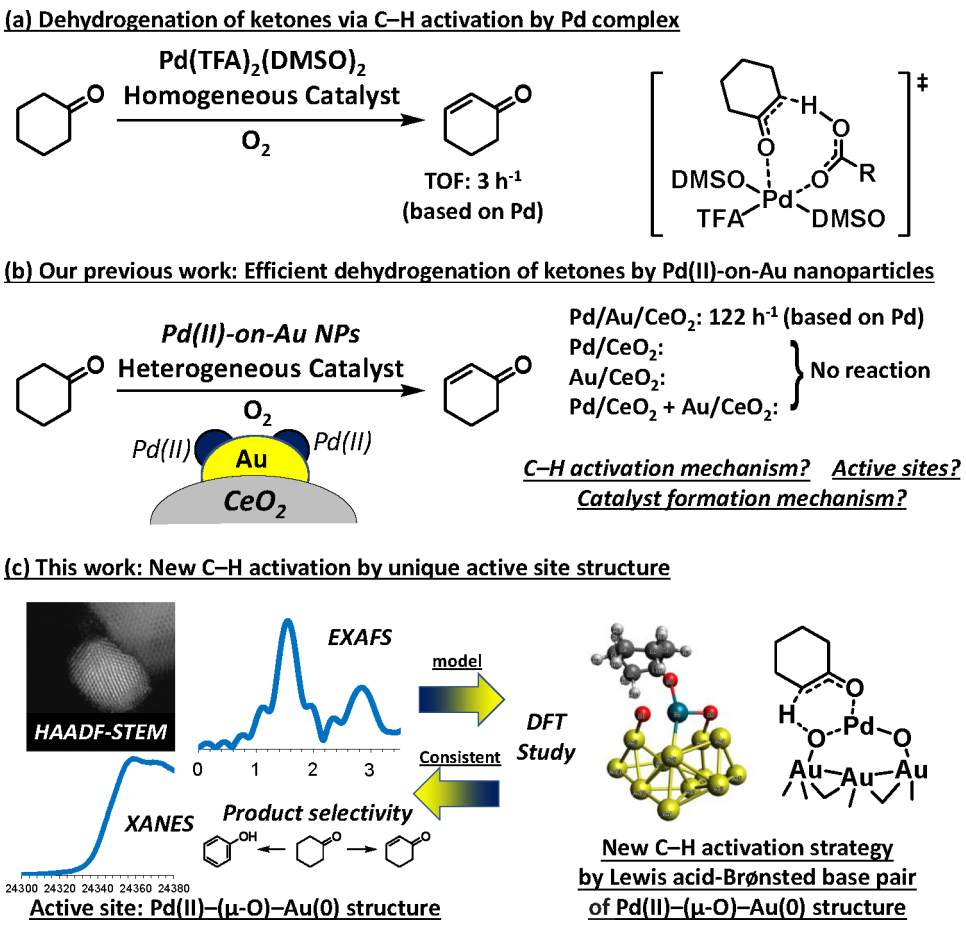

Figure 1. Examples of homogeneously or heterogeneously catalyzed cyclohexanone dehydrogenation and overview of this study.

have been rarely considered. This may be because experimentally determining the exact active site structures of supported catalysts is quite difficult, which forces calculations to consider various active site models as possibilities. Our previous work on the Au-catalyzed α,β-dehydrogenation of 1-methyl-4-piperidone was computationally expensive because our use of various Au cluster models forced us to consider many adsorption sites for O_2 to cleave C–H bonds.[38] Also, oversimplifying the model of supported nanoparticle catalysts may result in conclusions that are inconsistent with reality. To elucidate the mechanism and establish a design strategy for heterogeneous catalysts, an established active site structure-catalyzed important elementary reaction such as C–H bond activation needs to be considered based on multiple aspects combined with experimental and theoretical approaches.

Direct aerobic dehydrogenation of saturated ketones to α,β-unsaturated ketones, which are present in bioactive substances and versatile organic synthetic intermediates, is an attractive transformation via C–H bond activation.[39−43] Stahl et al. reported that the homogeneous Pd catalyst Pd-$(TFA)_2(DMSO)_2$ (TFA: trifluoroacetic acetate, DMSO: dimethyl sulfoxide) promotes the selective dehydrogenation of saturated ketones to α,β-unsaturated ketones including cyclohexanone.[39] They investigated the reaction mechanism in detail and assumed that the reaction proceeds via a five-coordinate transition structure through C–H cleavage by the TFA (or acetate) ligand (Figure 1a).[40] In the supposed mechanism of C–H activation, the Pd active site as a Lewis acid and an oxygen atom of the TFA (or acetate) ligand not directly coordinated to Pd as a Brønsted base simultaneously activate the C–H bond.[40] Recently, our group realized heterogeneously catalyzed aerobic α,β-dehydrogenation of saturated ketones including cyclohexanone by using Pd(II) species-on-Au(0) nanoparticles supported on CeO_2 (Pd/Au/CeO_2) (Figure 1b).[43] This system not only is environmentally benign but also exhibits a turnover frequency (TOF) (for cyclohexanone dehydrogenation) per Pd that exceeded those of previously reported homogeneous Pd catalysts[39−41] (122 vs 2−3 h^{-1}). Considering their turnover-limiting steps are the same: α-C–H bond activation,[40,43] the active site possessed by Pd/Au/CeO_2 is more effective than that of Pd-$(TFA)_2(DMSO)_2$ for C–H bond activation. We found it noteworthy that Au/CeO_2 (supported Au(0) nanoparticles), Pd/CeO_2 (supported Pd(0) nanoparticles, Pd(II) hydroxides, or Pd(II) oxides), or a physical mixture of Au/CeO_2 and Pd/CeO_2 did not catalyze this dehydrogenation. However, we were previously unable to clarify the details of the true active site structure in Pd/Au/CeO_2 and an efficient C–H bond activation mechanism.

In the present study, we focused on elucidating the C–H bond activation mechanism in the Pd/Au/CeO_2-catalyzed aerobic dehydrogenation of saturated ketones to α,β-unsaturated ketones. We used multiple approaches to investigate which active site structures unique to heterogeneous catalysts are effective at C–H bond activation for the dehydrogenation of cyclohexanone (Figure 1c). We performed experiments to analyze the reaction mechanism and characterize catalysts. Based on the experimental information, we

https://doi.org/10.1021/jacsau.1c00433
JACS Au 2022, 2, 394−406

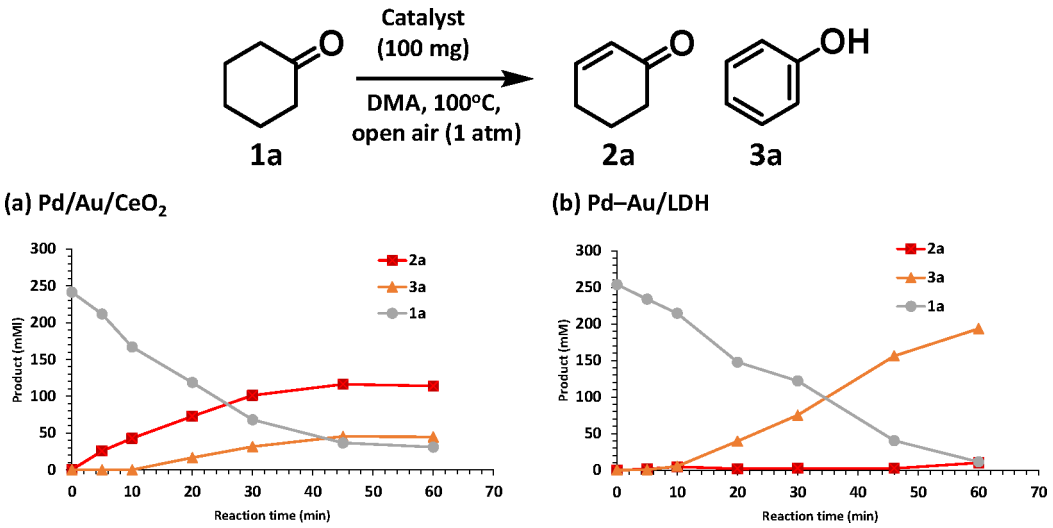

Figure 2. Reaction profiles of the **1a** dehydrogenation to **2a** and **3a** using (a) $Pd/Au/CeO_2$ or (b) Pd–Au/LDH as the catalyst. Reaction conditions: **1a** (0.5 mmol), catalyst (100 mg, Pd: 0.4 mol %, Au: 2.1 mol %), DMA (2 mL), 100 °C, open air (1 atm).

performed theoretical calculations with a suitable catalyst model.

EXPERIMENTAL METHODS

Preparation of $Pd/Au/CeO_2$

The $Pd/Au/CeO_2$ catalyst was prepared according to the method presented in our previous report.[43] CeO_2 (2 g) was added to an aqueous solution (60 mL) of $HAuCl_4$ (6.25 mM) and K_2PdCl_4 (0.83 mM), which was generated *in situ* from a mixture of $PdCl_2$ (8.9 mg, 0.05 mmol) and KCl (7.5 mg, 0.1 mmol). The slurry was stirred for 15 min, which was followed by dropping of aqueous NaOH (1 M) until the pH reached 10. After being stirred at room temperature (~25 °C) for 24 h, the resulting mixture was filtered, washed with deionized water (1 L), and dried *in vacuo* to afford the supported Pd–Au hydroxide precursor of $PdAu(OH)_x/CeO_2$. The Pd–Au hydroxide precursor (2 g) was dispersed in 50 mL of water and treated with $NaBH_4$ (70 mg, 1.85 mmol) at room temperature. The resulting slurry was then stirred vigorously at room temperature for 2 h under open-air conditions. The solid was then filtered off, washed with water (1 L), and dried *in vacuo* overnight to yield $Pd/Au/CeO_2$ as a dark-gray powder (2.1 wt % Au and 0.21 wt % Pd as determined by inductively coupled plasma atomic emission spectroscopy (ICP-AES)). An Mg–Al layered double hydroxide (LDH, $Mg_6Al_2(OH)_{16}CO_3{\cdot}4H_2O$) was used as the support to prepare Pd–Au/LDH in the same manner (2.5 wt % Au and 0.26 wt % Pd as determined by ICP-AES).

Preparation of $Pd/Au/CeO_2$-water

The $Pd/Au/CeO_2$-water catalyst was prepared as follows. First, $PdAu(OH)_x/CeO_2$ (1 g) was reduced with $NaBH_4$ (35 mg, 0.93 mmol) in water (25 mL) in an Ar atmosphere at room temperature. After 2 h, the solid was filtered off, washed with ethanol (25 mL), and dried *in vacuo* to afford $Pd/Au/CeO_2$-Ar. Then, $Pd/Au/CeO_2$-Ar (200 mg) was stirred with water (5 mL) in an air atmosphere for 2 h. The solid was filtered off and washed with water (200 mL) to obtain $Pd/Au/CeO_2$-water (2.6 wt % Au and 0.22 wt % Pd as determined by ICP-AES).

Preparation of $Pd/Au/CeO_2$-air

The $Pd/Au/CeO_2$-air catalyst was obtained by exposing $Pd/Au/CeO_2$-Ar to an air atmosphere for more than 2 h (2.9 wt % Au and 0.23 wt % Pd as determined by ICP-AES).

Catalytic Reactions

We placed a catalyst (100 or 50 mg), cyclohexanone (0.5 mmol), biphenyl (internal standard), *N*,*N*-dimethylacetamide (DMA) or toluene (2 mL), and a Teflon-coated magnetic stir bar in a Pyrex glass reactor (volume of ~20 mL). Then, the mixture was stirred at 70 or 100 °C in an air atmosphere. The conversion and product yields were determined by gas chromatography. The same procedure was used for analysis of the reaction kinetics. Sampling was performed 1, 2, 3, 4, and 5 min after the start of the reaction, and the data were used to determine the initial reaction rate with each catalyst.

Catalyst Characterization

The particle sizes and distributions of the catalysts were measured by high-angle annular dark-field scanning transmission electron microscopy (HAADF-STEM) using a JEOL JEM-ARM200F instrument equipped with energy-dispersive X-ray spectrometry (EDS) at 200 kV. X-ray absorption spectroscopy (XAS) of the Pd K-edge and Au L_3-edge was carried out by using the transmission and fluorescence method at the BL14B2 beamline of SPring-8. The X-ray beam was monochromatized by using a single pair of Si(311) crystal monochromators. The energy was calibrated by using a Pd metal foil for the Pd K-edge XAS and an Au metal foil for the Au L_3-edge XAS. X-ray absorption near-edge structure (XANES) and extended X-ray absorption fine structure (EXAFS) data were analyzed by using Athena and Artemis software (Demeter, ver. 0.9.025; Bruce Ravel). The k^3-weighed EXAFS spectra were Fourier-transformed into *R*-space at 3–13 $Å^{-1}$. Details on the XAFS measurement methods and EXAFS analyses are summarized in the Supporting Information.

Density Functional Theory Calculation

We used Gaussian16[44] as the calculation software, M06[45] as the exchange–correlation functional, the Stuttgart/Dresden basis set (SDD)[46] with the effective core potential for Au and Pd, and 6-31G(d,p)[47] as the basis sets for the other elements. M06 is an exchange–correlation functional often used in systems with transition metals especially Au,[38,48,49] and SDD is a basis set often used in systems with Au or Pd.[38,50,51] The solvent effect was calculated with a conductor-like polarizable continuum model using toluene. The transition state structures contained one imaginary frequency exhibiting atom displacements along the expected reaction pathway. The optimized structure for the reactant, intermediate, and product states contained no imaginary frequency. Structures of transition states, the corresponding reactants, and the corresponding products were connected by intrinsic reaction coordinate calculations. Pictures of each structure were drawn by using the software Avogadro. The Cartesian coordinates of the calculated structures are given in the Supporting Information.

https://doi.org/10.1021/jacsau.1c00433
JACS Au 2022, 2, 394–406

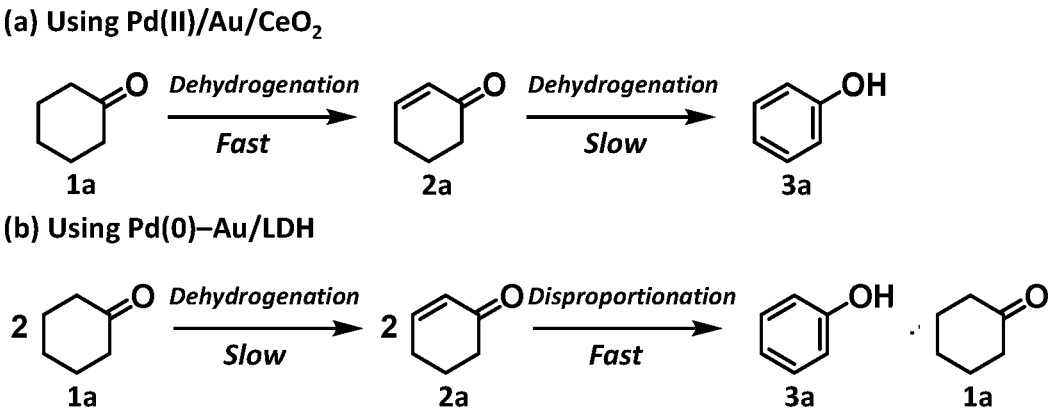

Figure 3. Reaction paths of **1a** to **3a** via **2a** catalyzed by (a) Pd(II)/Au/CeO_2 or (b) Pd(0)–Au/LDH.

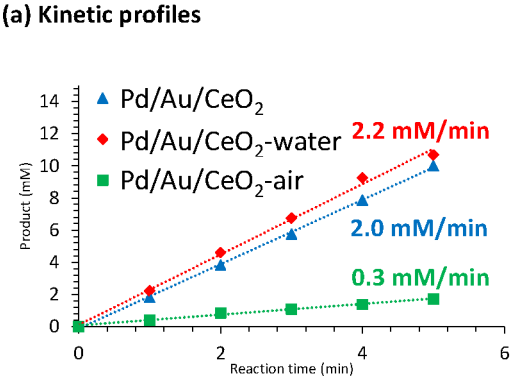

(b) Catalyst effects

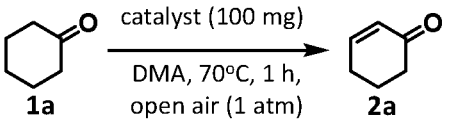

catalyst	Yield of 2a (%)
Pd/Au/CeO_2	56
Pd/Au/CeO_2-water	43
Pd/Au/CeO_2-air	9

Figure 4. (a) Kinetic profiles and (b) catalyst effects for the **1a** dehydrogenation using Pd/Au/CeO_2, Pd/Au/CeO_2-water, or Pd/Au/CeO_2-air. Reaction conditions of (a): **1a** (0.5 mmol), catalyst (50 mg, Pd: 0.2 mol %, Au: 1.1 mol %), DMA (2 mL), 70 °C, open air (1 atm). Reaction conditions of (b): **1a** (0.5 mmol), catalyst (100 mg, Pd: 0.4 mol %, Au: 2.1 mol %), DMA (2 mL), 70 °C, open air (1 atm), 1 h.

RESULTS AND DISCUSSION

Active Species Estimation from Reactions Using Various Catalysts

In our previous study, we found that a Pd/Au/CeO_2 catalyst is effective for the selective α,β-dehydrogenation of various saturated ketones including cyclohexanone and can be prepared via the deposition-precipitation of Pd and Au hydroxides on CeO_2 ($PdAu(OH)_x/CeO_2$) followed by $NaBH_4$ treatment in water and an air atmosphere.[43] As with Pd–Au catalysts prepared in the same manner on other supports such as Al_2O_3[52,53] and Mg–Al LDH,[54] the STEM-EDS mapping of Pd/Au/CeO_2 showed that Pd–Au bimetallic nanoparticles were highly dispersed on the CeO_2 support (Figure S1).[43] Surprisingly, however, the XANES and XPS results revealed that the Pd and Au species in Pd/Au/CeO_2 had valences of two and zero, respectively, which suggests the formation of Pd(II)-on-Au(0) nanoparticles.[43] In contrast, the same $NaBH_4$ treatment of Pd and Au hydroxide precursors on Al_2O_3[43,53] and LDH[55] afforded mainly Pd(0)–Au(0) alloy nanoparticles (Figures S2 and S3). In fact, Pd/Au/CeO_2 showed a uniquely higher catalytic activity for selective α,β-dehydrogenation of cyclohexanone at 70 °C than supported Pd(0)–Au(0) alloy nanoparticle catalysts,[43] which can be attributed to the unique Pd(II)-on-Au(0) nanoparticle structure of Pd/Au/CeO_2. On the other hand, the XANES results for Pd/Au/CeO_2 revealed the formation of Pd(0) species during the reaction.[43] Given our previous report on the dehydrogenative aromatization of cyclohexanones to phenols at 130 °C using a Pd(0)–Au(0) alloy catalyst supported on LDH (Pd–Au/LDH) via aerobic α,β-dehydrogenation of cyclohexanones to 2-cyclohexen-1-ones,[54,55] the Pd(0) species formed in Pd/Au/CeO_2 may be the true active species.

To establish whether the true active species in Pd/Au/CeO_2 for dehydrogenation is Pd(II) or Pd(0), we investigated the differences between Pd/Au/CeO_2 and Pd–Au/LDH in terms of the product selectivity for the dehydrogenation of cyclohexanone (**1a**) to form 2-cyclohexen-1-one (**2a**) and phenol (**3a**) at 100 °C (Figure 2). For Pd/Au/CeO_2, **3a** was produced via a typical sequential dehydrogenation from **1a** to **3a** via **2a**, and the formation of **2a** from **1a** was at a faster rate than that of **3a** from **2a** (Figure 2a). In fact, the dehydrogenation to **3a** from **2a** proceeded quite slowly (Figure S4a). For Pd–Au/LDH, **3a** was selectively synthesized with almost no detection of **2a** as an intermediate, which suggests that the formation of **3a** from **2a** was much faster than that of **2a** from **1a** (Figure 2b). Pd(0) nanoparticle catalysts including Pd–Au/LDH are known to quickly produce phenols by the disproportionation reaction of 2-cyclohexen-1-ones.[54,42] In the present case, the quick disproportionation to **3a** and **1a** was also observed when the reaction started from **2a** using Pd–Au/LDH (Figure S4b). Therefore, the active site of Pd/Au/CeO_2 containing Pd(II) species was highly effective for the α,β-dehydrogenation of cyclohexanones to 2-cyclohexen-1-ones but less active for the sequential dehydrogenation to phenols (Figure 3a). This is clearly different from that of Pd–Au/LDH mainly containing Pd(0) species, which showed low activity for α,β-dehydrogenation and caused the efficient disproportiona-

https://doi.org/10.1021/jacsau.1c00433
JACS Au 2022, 2, 394–406

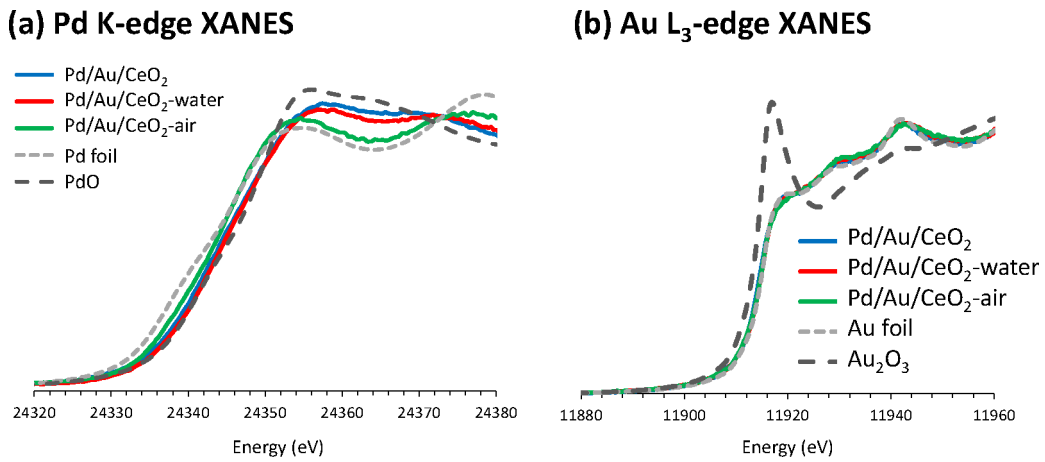

Figure 5. (a) Pd K-edge XANES and (b) Au L_3-edge XANES spectra of $Pd/Au/CeO_2$, $Pd/Au/CeO_2$-water, $Pd/Au/CeO_2$-air, and references.

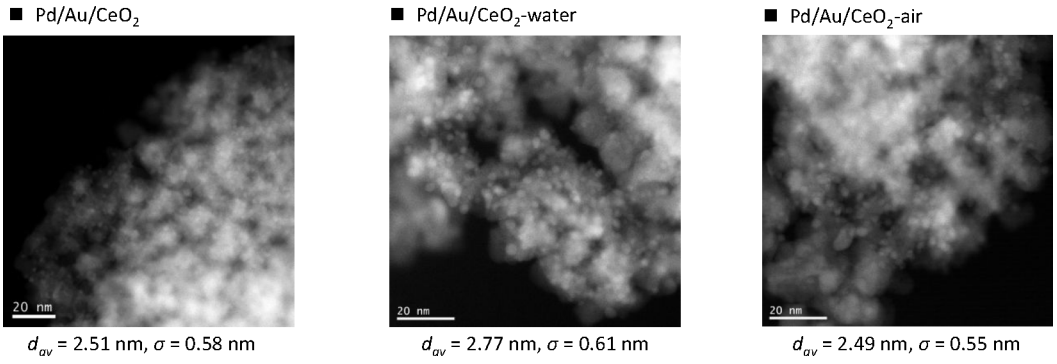

Figure 6. HAADF-STEM images of $Pd/Au/CeO_2$, $Pd/Au/CeO_2$-water, and $Pd/Au/CeO_2$-air. The average sizes of nanoparticles (d_{av}) and standard deviations (σ) are given below the images.

tion of 2-cyclohexen-1-ones to phenols and cyclohexanones (Figure 3b). Based on these results, we concluded that the active species for the $Pd/Au/CeO_2$ catalysis of α,β-dehydrogenation is not the Pd(0) species formed during the reaction but the Pd(II)-on-Au(0) nanoparticles.

However, the detailed active site structure of the Pd(II) species in $Pd/Au/CeO_2$ and its formation mechanism have not yet been elucidated. To clarify the active site structure and formation mechanism of Pd(II)-on-Au(0) nanoparticles on CeO_2, two types of controlled Pd−Au catalysts supported on CeO_2 were designed. We previously prepared $NaBH_4$-treated Pd and Au hydroxides supported on CeO_2 in an Ar atmosphere (i.e., $Pd/Au/CeO_2$-Ar), which had a Pd valence of zero (Figure S5).[43] In the present study, we prepared (i) air-exposed $Pd/Au/CeO_2$-Ar (i.e., $Pd/Au/CeO_2$-air) and (ii) water-treated $Pd/Au/CeO_2$-Ar in an open-air atmosphere (i.e., $Pd/Au/CeO_2$-water). Then, the catalytic activities of $Pd/Au/CeO_2$, $Pd/Au/CeO_2$-water, and $Pd/Au/CeO_2$-air for the aerobic α,β-dehydrogenation of **1a** to **2a** at 70 °C in DMA were compared under an air atmosphere (Figure 4). Under an Ar atmosphere, $Pd/Au/CeO_2$ did not afford any products, showing that O_2 works as the terminal oxidant. Under the aforementioned conditions in an air atmosphere, **2a** was selectively obtained without the formation of **3a**, regardless of which catalyst was used. The initial production rate of **2a** with $Pd/Au/CeO_2$ (2.0 mM/min) was similar to that with $Pd/Au/CeO_2$-water (2.2 mM/min), whereas that with $Pd/Au/CeO_2$-air was quite low (0.33 mM/min) (Figure 4a). A similar trend was observed for the **2a** yields 1 h after the start of the reaction (Figure 4b). These results suggest that $Pd/Au/CeO_2$ and $Pd/Au/CeO_2$-water may have similar active site structures effective for the dehydrogenation reaction, in contrast to that of $Pd/Au/CeO_2$-air.

Characterization of Catalysts

To clarify the active site structure for dehydrogenation, the catalysts of $Pd/Au/CeO_2$, $Pd/Au/CeO_2$-water, $Pd/Au/CeO_2$-air, and $Pd/Au/CeO_2$-Ar were characterized with various methods. The Pd K-edge XANES spectra of $Pd/Au/CeO_2$ and $Pd/Au/CeO_2$-water were almost the same as that of PdO (Figure 5a), which indicates that their Pd species were mostly bivalent. In contrast, the spectrum of $Pd/Au/CeO_2$-air was relatively close to that of $Pd/Au/CeO_2$-Ar, which indicates that the valence of Pd was almost zero, although there was a small amount of the Pd(II) species (Figures 5a and S5). The Au L_3-edge XANES spectra of $Pd/Au/CeO_2$, $Pd/Au/CeO_2$-water, and $Pd/Au/CeO_2$-air were almost consistent with that of the Au foil (Figure 5b). These results indicate that the immobilized Pd(II) and Au(III) species in the hydroxide precursor via deposition-precipitation ($PdAu(OH)_x/CeO_2$) were reduced to Pd(0) and Au(0) species by the $NaBH_4$ treatment. Eventually, the Pd(II) and Au(0) species formed through selective oxidation of the Pd(0) species by exposure to water in an air atmosphere. Considering previous reports[43,53] and the case of Pd−Au/LDH,[55] the oxidation of Pd(0) to Pd(II) in the presence of Au(0) is a unique phenomenon when CeO_2 is the support. These results and the fact that cosupported Pd(II) and Au(0) species are indispensable for α,β-dehydrogenation (Figure 1b) suggest that the catalytic

https://doi.org/10.1021/jacsau.1c00433
JACS Au 2022, 2, 394−406

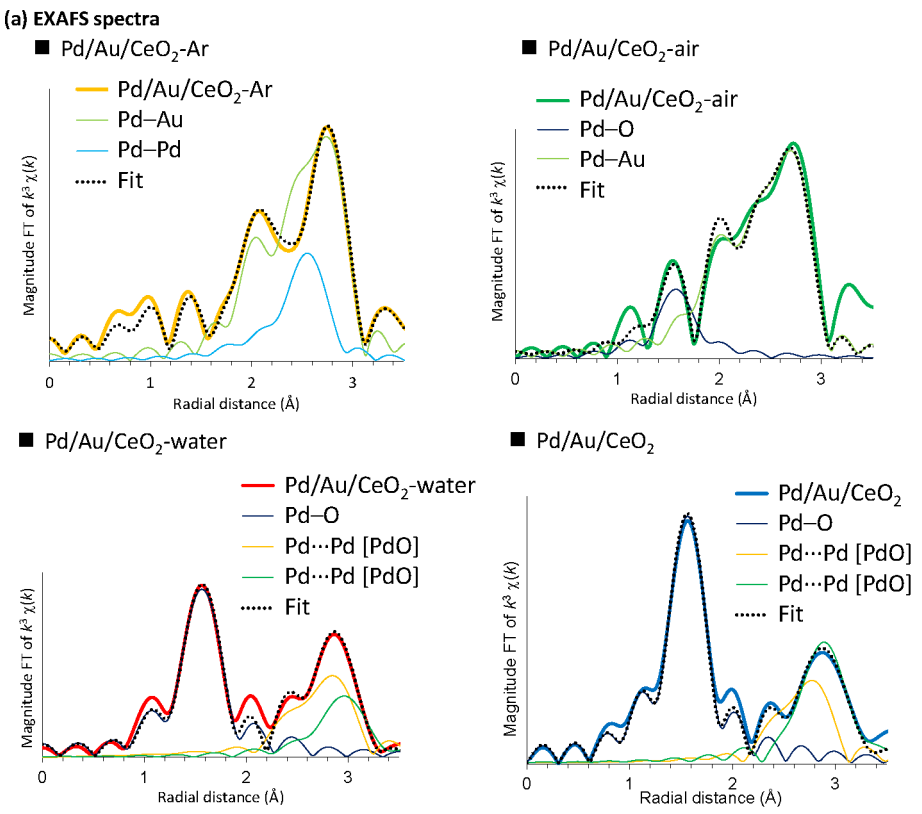

(b) Fitting parameters

■ Pd/Au/CeO_2-Ar

Shell	CN	R (Å)	ΔE_{j0} (eV)	σ^2 (Å^2)	R_f(-)
Pd–Au	6.28± 0.69	2.82	−1.41	0.00981	0.00928
Pd–Pd	1.49± 0.39	2.82	−4.57	0.0101	

■ Pd/Au/CeO_2-air

Shell	CN	R (Å)	ΔE_{j0} (eV)	σ^2 (Å^2)	R_f(-)
Pd–O	0.36± 0.17	2.02	−0.93	0.00032	0.0238
Pd–Au	7.90± 1.05	2.81	−5.67	0.01127	

■ Pd/Au/CeO_2-water

Shell	CN	R (Å)	ΔE_{j0} (eV)	σ^2 (Å^2)	R_f(-)
Pd–O	1.96± 0.12	2.02	4.93	0.00170	
Pd···Pd [PdO]	1.25± 0.14	3.01	12.56	0.00485	0.0203
Pd···Pd [PdO]	2.18± 0.36	3.30	−11.13	0.00821	

■ Pd/Au/CeO_2

Shell	CN	R (Å)	ΔE_{j0} (eV)	σ^2 (Å^2)	R_f(-)
Pd–O	2.36± 0.08	2.00	3.90	0.00141	
Pd···Pd [PdO]	0.92± 0.09	2.95	13.93	0.00455	0.0108
Pd···Pd [PdO]	1.71± 0.12	3.25	−14.12	0.00435	

Figure 7. (a) Pd K-edge EXAFS spectra and (b) fitting parameters of Pd/Au/CeO_2-Ar, Pd/Au/CeO_2-air, Pd/Au/CeO_2-water, and Pd/Au/CeO_2.

active site structure in Pd/Au/CeO_2 comprises both Pd(II) and Au(0) species.

HAADF-STEM analyses revealed that the average nanoparticle sizes in Pd/Au/CeO_2, Pd/Au/CeO_2-water, and Pd/Au/CeO_2-air were 2.51, 2.77, and 2.49 nm, respectively. Thus, the particle sizes of all catalysts were almost the same (Figures 6 and S6). Therefore, the difference in activity of these catalysts cannot be attributed to the particle size. The HAADF-STEM images of Pd/Au/CeO_2 showed some particles with a bright center and dark peripheral region (Figure S7). The observed lattice spacings at the center of the particles were 2.31 and 2.36 Å; this is almost identical to the lattice spacing for the (111) plane of Au, which is 2.35 Å.[56] In contrast, the lattice spacings of the peripheral region of the particle were 2.62 and 2.02 Å; they are almost identical to the lattice spacings for the (101) and (111) planes of PdO, which are 2.64 and 2.00 Å, respectively.[57] These results indicate that bimetallic PdO-on-Au(0) nanoparticles were present in Pd/

https://doi.org/10.1021/jacsau.1c00433
JACS Au 2022, 2, 394−406

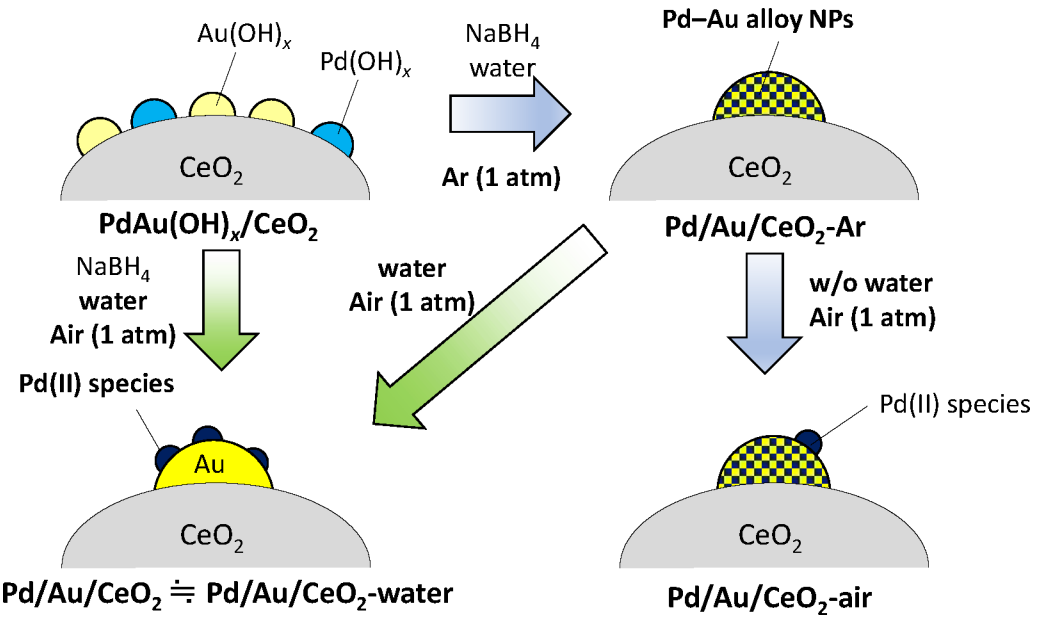

Figure 8. Possible formation mechanism of the active site structure.

Au/CeO_2. Also, a nanoparticle which does not possess a clear PdO nanodomain with the lattice spacing attributed to (111) plane of Au was also observed in $Pd/Au/CeO_2$ using HAADF-STEM (Figure S7). As for such a nanoparticle, considering the XANES spectrum showing that Pd species were mostly bivalent in $Pd/Au/CeO_2$ (Figure 5a) and the STEM-EDS mappings showing that most of the nanoparticles consisted of both Au and Pd (Figure S1), PdO nanospecies were probably dispersed on an Au nanoparticle without forming PdO nanodomains.

Next, we attempted to clarify the fine structure of the active site and its formation mechanism by Pd K-edge EXAFS analysis. Figure 7a shows the spectra of $Pd/Au/CeO_2$-Ar, $Pd/Au/CeO_2$-air, $Pd/Au/CeO_2$-water, and $Pd/Au/CeO_2$ as well as the fitted curves. Figure 7b summarizes the structural parameters obtained from the curve fitting analysis. We performed a curve fitting analysis on $Pd/Au/CeO_2$-Ar, and the spectrum was successfully reproduced by using a Pd−Pd shell derived from the Pd foil and a Pd−Au shell derived from an alloy model of Au nanoparticles with Pd substitution. This suggests that Pd in $Pd/Au/CeO_2$-Ar mainly forms disordered alloys with Au. In the EXAFS spectrum of $Pd/Au/CeO_2$-air, a small peak that may have derived from Pd−O was observed around 1.4 Å. The presence of a small amount of Pd(II) species was also confirmed by the XANES analysis described above. The EXAFS spectrum of $Pd/Au/CeO_2$-air could be reproduced by using a Pd−O shell derived from PdO and the Pd−Au shell. Therefore, the Pd(0) species in $Pd/Au/CeO_2$-Ar is partially oxidized to Pd(II) by exposure to air, while the rest exists mainly as an alloy with Au even after this treatment. The shapes of the EXAFS spectra of $Pd/Au/CeO_2$-water and $Pd/Au/CeO_2$ were significantly different from those of $Pd/Au/CeO_2$-Ar and $Pd/Au/CeO_2$-air. $Pd/Au/CeO_2$-water and $Pd/Au/CeO_2$ clearly had a peak originating from Pd−O around 1.4 Å, while the peaks from the metal−metal bonds were mostly absent. The peak around 2.8 Å may have originated from longer-range Pd···Pd interactions in the PdO structure. We successfully reproduced these EXAFS spectra by using the Pd−O shell and two Pd···Pd shells originating from PdO. As a result, the coordination number (CN) of Pd−O (2.36) in $Pd/Au/CeO_2$ is comparatively small, suggesting that the average size of PdO in $Pd/Au/CeO_2$ is likely smaller than that of the aforementioned PdO nanodomains observed by HAADF-STEM (Figure S7).

Because the catalysts with only Pd(II) species supported on CeO_2 did not show any activity for the present dehydrogenation, the Pd−O−Pd and Pd−O−Ce structures were not considered to be effective for the reaction. In other words, the activity of PdO itself and the effect of the CeO_2 support were considered negligible. Additionally, the STEM and EXAFS analysis of $Pd/Au/CeO_2$ revealed the possible presence of PdO nanospecies-on-Au nanoparticles (Figure S7). Thus, we hypothesized that a Pd(II)−(μ-O)−Au(0) structure generated at the nanoparticle interface between PdO and Au(0) would play an important role in this reaction. We compared the imaginary parts of the Fourier transforms of $Pd/Au/CeO_2$ and PdO in detail and found that they deviated at R = 1.2−1.9 Å and R = 2.7−3.0 Å (Figure S8). We considered that the above hypothesis is not wrong because such a shift in imaginary parts is frequently observed when another element is substituted in metal oxides.[58−63]

As summarized in Figure 7b, the CNs of Pd−O in $Pd/Au/CeO_2$ (2.36) and $Pd/Au/CeO_2$-water (1.96) were almost the same, while that of $Pd/Au/CeO_2$-air (0.36) was clearly much smaller. A good correspondence between the order of catalytic activity and the CN was obtained (Figure 4): the catalytic activity increased with the amount of the Pd−O species. Considering the aforementioned imaginary Fourier shift suggesting that the CNs of Pd−O could mainly arise from Pd(II)−(μ-O)−Au(0) structure, this correlation is consistent with our assumption that Pd(II)−(μ-O)−Au(0) structure is the catalytic active site.

Based on the above experimental evidence, we concluded that the Pd(II)−(μ-O)−Au(0) structure generated at the interface of PdO-on-Au nanoparticles is probably the true active site for the present dehydrogenation. When we compared the product selectivity of cyclohexanone dehydrogenation using $Pd/Au/CeO_2$ with that using Pd−Au/LDH,

https://doi.org/10.1021/jacsau.1c00433
JACS Au 2022, 2, 394−406

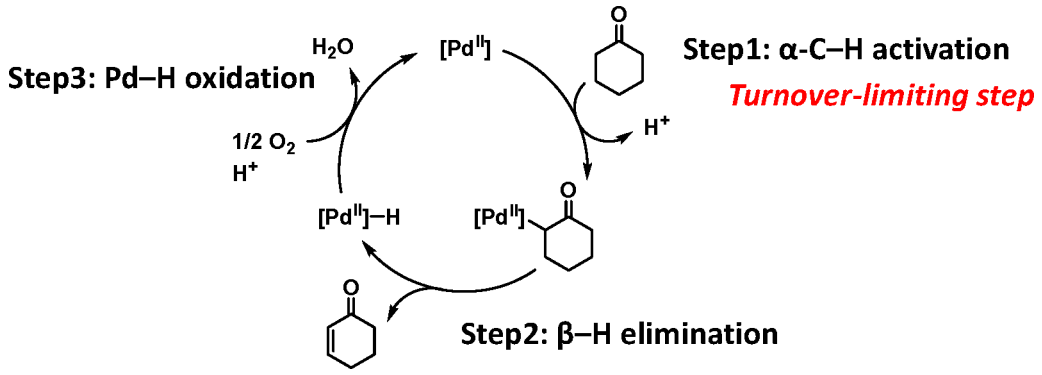

Figure 9. Proposed catalytic cycle for the α,β-dehydrogenation of cyclohexanone.

the active site of Pd/Au/CeO_2 appeared to be the Pd(II) species rather than the Pd(0) species. Catalytic activity tests and XANES spectra revealed that the Pd(II) species with Au(0) in Pd/Au/CeO_2 is included in the active site structure. HAADF-STEM images showed the presence of bimetallic PdO-on-Au(0) nanoparticles in Pd/Au/CeO_2. EXAFS analysis indicated that the Pd(II)−(μ-O)−Au(0) structure may exist in Pd/Au/CeO_2 and that the CNs of Pd−O with Au(0) nanoparticles have a positive correlation with the catalytic activity for α,β-dehydrogenation. The presence of Pd(II)−(μ-O)−Au(0) structure as the active site for the dehydrogenation is comprehensively supported by all of the experimental data.

We propose a formation mechanism for the active site structure based on the results of the above experiments using controlled catalysts (Figure 8). The Pd(II)−(μ-O)−Au(0) structure cannot be obtained by reducing the Pd−Au hydroxide precursor on CeO_2 ($PdAu(OH)_x/CeO_2$) using $NaBH_4$ in the absence of O_2. Although mere exposure of Pd/Au/CeO_2-Ar to air does not sufficiently oxidize the Pd(0) species, treatment of Pd/Au/CeO_2-Ar with water in an air atmosphere afforded the Pd(II)−(μ-O)−Au(0) structure, which was almost the same as that of Pd/Au/CeO_2. Thus, the $NaBH_4$ treatment of $PdAu(OH)_x/CeO_2$ in water and in an air atmosphere causes the formation of Pd(0)−Au(0) alloy nanoparticles followed by the selective full oxidation of Pd(0) species to Pd(II) oxides on the Au(0) nanoparticles, which constructs a significant amount of the active Pd(II)−(μ-O)−Au(0) structure. Importantly, the use of CeO_2 as the support is essential for the formation of this active site structure in the selective Pd(0) oxidation step. Even if the Pd−Au hydroxide precursor is treated in the same manner on other supports such as Al_2O_3 or LDH, this produces inactive Pd(0)−Au(0) alloy nanoparticles instead of an effective structure for α,β-dehydrogenation.

Density Functional Theory Calculations

Our previous experimental results showed that the Pd(II)−(μ-O)−Au(0) structure is probably the active site for cyclohexanone dehydrogenation. We used density functional theory (DFT) to calculate how cyclohexanone is activated on this active site and how the dehydrogenation to 2-cyclohexen-1-one proceeds. Based on previous reports,[39−42] we performed the following experiments and calculations under the assumption that the reaction proceeds according to the following catalytic cycle (Figure 9):

(1) A Pd(II)-enolate species is formed via the α-C−H bond activation of cyclohexanone.

(2) The enolate species undergoes typical β-hydride elimination to afford 2-cyclohexen-1-one and a Pd(II)-hydride species.

(3) The hydride species is then oxidized by O_2.

A kinetic isotope effect was clearly observed (k_H/k_D = 2.2) for cyclohexanone and cyclohexanone-α-d_4 but not for cyclohexanone-α-d_4 and cyclohexanone-d_{10} (k_H/k_D = 1.1).[43] Furthermore, the reaction rates were almost independent of the partial pressure of O_2 at 0.1−0.4 atm.[43] Therefore, the turnover-limiting step clearly involves cleavage of the α-C−H bond. Based on the Arrhenius plot for the effect of the reaction temperature on Pd/Au/CeO_2-catalyzed cyclohexanone dehydrogenation in toluene (Figures S9 and S10), the apparent activation energy is 11.3 kcal/mol.

For DFT calculations, we first constructed a model of the structure of the catalytic active site. The experimental results suggested the formation of a heterometallic μ-oxo structure of Pd(II)−(μ-O)−Au(0). Thus, we constructed a $Pd_1O_2Au_{12}$ structure by replacing the Au atom at the vertex with Pd and placing an O atom in the middle of the adjacent Au atom by referring to the Au_{13} structure of Au/CeO_2 reported previously.[64] Because the XANES analysis confirmed that the electronic state of Au in Pd/Au/CeO_2 was identical to that of the Au foil (Figure 5b), we supposed that there was no electron transfer between the nanoparticles and CeO_2. Therefore, we set the charge of the model cluster to zero. After optimizing the cluster model structures with different spin multiplicities of singlet, triplet, and quintet, we found the singlet structure **1** to be the most stable (Figure S11).

We then used this $Pd_1O_2Au_{12}$ model **1** to investigate the dehydrogenation mechanism of cyclohexanone to 2-cyclohexen-1-one (Figure 10a).[65] When cyclohexanone was brought into close proximity to the cluster, we found a stable adsorption structure **1**-**1** (Figure S12). The adsorption proceeded exothermally, and the adsorption energy was calculated to be 6.3 kcal/mol. The C═O bond distance of cyclohexanone before adsorption was 1.215 Å, which was lengthened to 1.232 Å by adsorption on the Pd atom. Furthermore, one of the α-H atoms of the adsorbed cyclohexanone molecule was at a distance (2.405 Å) where it interacted with the O atom of the Pd(II)−(μ-O)−Au(0) structure, and its natural population analysis (NPA) charge (0.308) was larger than that of cyclohexanone substrate (0.278). From this adsorption structure, one can easily assumed that the cyclohexanone molecule is activated by the Lewis acid−Brønsted base pair site and that the α-H atom can be abstracted as a proton. We then investigated the reaction

https://doi.org/10.1021/jacsau.1c00433
JACS Au 2022, 2, 394−406

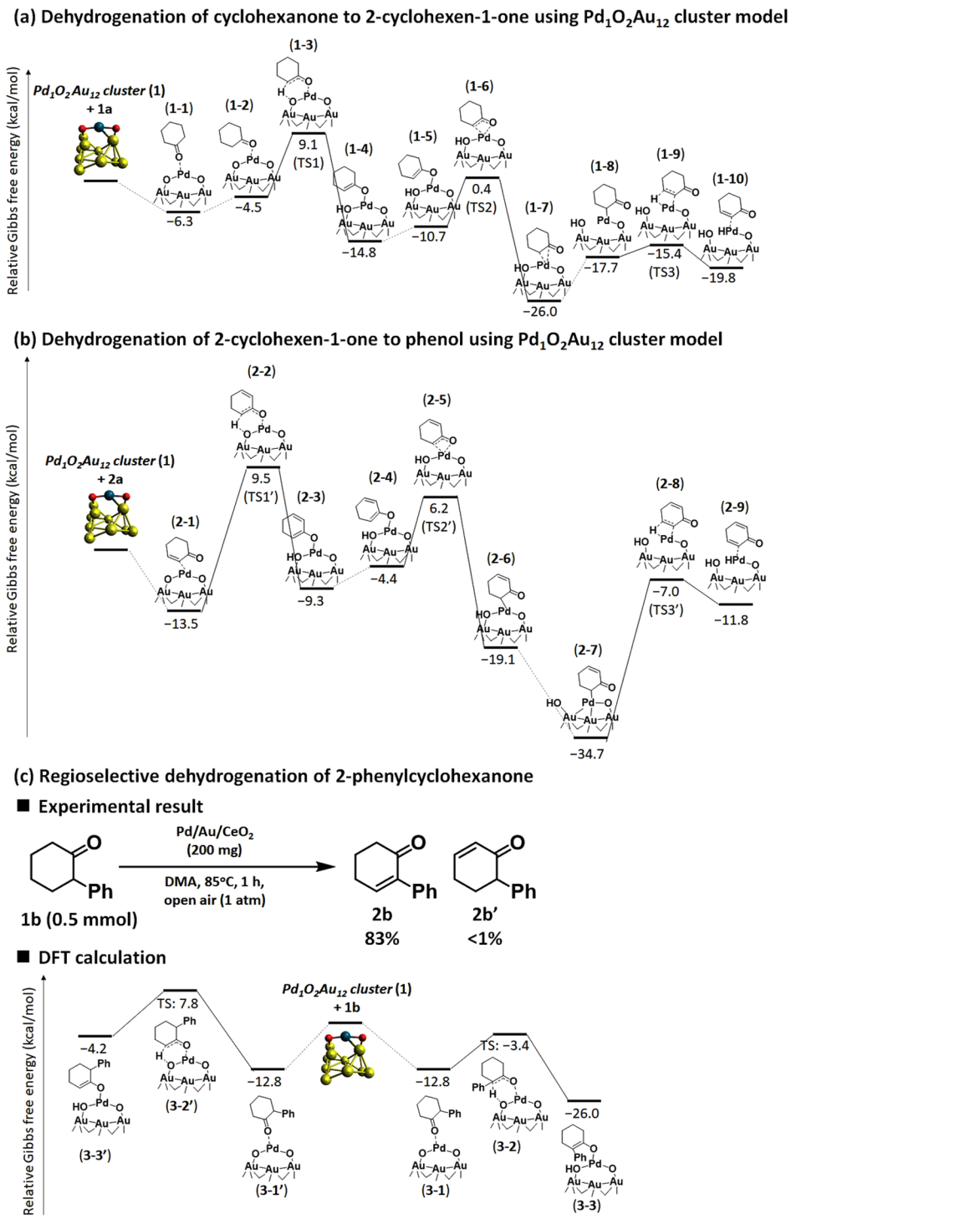

Figure 10. Optimized structures and transition states calculated using a $Pd_1O_2Au_{12}$ cluster model for the following pathways: (a) from cyclohexanone to 2-cyclohexen-1-one, (b) from 2-cyclohexen-1-one to phenol, and (c) from 2-phenylcyclohexanone. Yellow: gold, blue: palladium, red: oxygen.

pathway for the α-C−H bond cleavage of cyclohexanone from the adsorption structure and found a transition state (TS1) structure **1-3** in which the O atom of the Pd(II)−(μ-O)−Au(0) structure actually acts as a Brønsted base to deprotonate the α-H atom. The activation free energy for the reaction pathway **1-1** → **1-4** (free energy difference between **1-1** and **1-3**) was calculated to be 15.4 kcal/mol. In the intermediate state structure **1-4** after TS1, the carbonyl oxygen was coordinated to the Pd(II) species (*O*-enolate species) and the β-hydride elimination would not proceed from this *O*-enolate state. We investigated the formation of enolate species that could proceed the β-hydride elimination starting from the *O*-enolate species **1-4**. We successfully found a reasonable reaction pathway and a stable enolate species **1−7**. The activation free energy for the reaction pathway **1-4** → **1-7** (free energy difference between **1-4** and **1-6**) was calculated to be 15.2 kcal/mol. This value was smaller than that for the reaction pathway **1-1** → **1-4**, although only slightly. Calculations using

https://doi.org/10.1021/jacsau.1c00433
JACS Au 2022, 2, 394−406

this cluster model revealed that, once the enolate species **1-7** was generated, the subsequent β-hydride elimination step proceeded readily according to the reaction pathway **1-7** → **1-10** with the activation free energy of 10.6 kcal/mol (free energy difference between **1-7** and **1-9**). Although we did not calculate the reaction of the Pd(II)-hydride species with O_2, the above calculation results are consistent with the experimental results showing that the α-C−H bond cleavage is the turnover-limiting step. We considered the apparent activation energy obtained experimentally (11.3 kcal/mol) to be roughly reproduced by the present calculations.

The above DFT calculations indicate that the Pd(II) species acts as a Lewis acid to be coordinated by the carbonyl of cyclohexanone and that the μ-oxo species of the Pd(II)−(μ-O)−Au(0) structure acts as a Brønsted base to deprotonate the α-H of cyclohexanone. In this reaction mechanism, the Pd(II)−(μ-O)−Au(0) structure works as a neighboring Lewis acid−Brønsted base pair, which efficiently promotes the deprotonation via concerted catalysis.[66] This reaction mechanism is different from the deprotonation by ligands assumed for the homogeneous $Pd(TFA)_2(DMSO)_2$ catalyst,[40] where the O atom not coordinated to Pd in the ligand TFA acts as a Brønsted base to extract α-H atom of cyclohexanone. In the reaction mechanism of the Pd(II)−(μ-O)−Au(0) structure in our study, the O atom directly coordinated to Pd acts as a Brønsted base.[67] The concerted catalytic effect of the Lewis acid−Brønsted base pair site may be utilized to design heterogeneous catalysts with higher efficiency than homogeneous ones.

DFT calculations were also performed to support that the phenol formation from 2-cyclohexen-1-one at 70 °C is energetically unfavorable when $Pd/Au/CeO_2$ is used. Under the assumption that the reaction proceeds in the same manner as for cyclohexanone, similar transition states TS1′, TS2′, and TS3′ were found. The activation free energy was 27.7 kcal/mol for TS3′ (Figure 10b), which is significantly greater than the activation free energy for the α,β-dehydrogenation of cyclohexanone (15.4 kcal/mol) and is consistent with the experimental results showing that 2-cyclohexen-1-one was selectively generated at 70 °C without forming phenol.

Finally, DFT calculations were performed for the dehydrogenation of 2-phenylcyclohexanone (**1b**). When **1b** was dehydrogenated by using $Pd/Au/CeO_2$, the phenyl-substituted side was regioselectively dehydrogenated to give 2-phenyl-2-cyclohexen-1-one (**2b**), while the unsubstituted side was not dehydrogenated to 6-phenyl-2-cyclohexen-1-one (**2b′**) (Figure 10c).[43] We investigated whether the selectivity of this reaction could be explained by DFT calculations if we assume a reaction mechanism similar to that of cyclohexanone. The activation free energy in the deprotonation step was calculated to be 9.4 kcal/mol for the phenyl-substituted side (**3-1** → **3-3**) in contrast with 20.6 kcal/mol for the nonsubstituted side (**3-1′** → **3-3′**), which is sufficient to explain the regioselectivity in the reaction (Figure 10c). The difference in energy was attributed to the stability of the anion produced by the deprotonation of **1b**. This is stabilized by the resonance effect on the phenyl-substituted side, which lowers the transition state energy. Therefore, these calculations with the $Pd_1O_2Au_{12}$ structure model are also consistent with the product selectivity and regioselectivity of α,β-dehydrogenation using $Pd/Au/CeO_2$ and validate the C−H bond activation mechanism enabled by the Lewis acid−Brønsted base pair of the Pd(II)−(μ-O)−Au(0) structure.

CONCLUSION

Our experimental results and DFT calculations showed that the Pd(II)−(μ-O)−Au(0) structure leads to highly efficient α-C−H bond activation of cyclohexanone. The EXAFS results showed that the CN of Pd−O had a positive correlation with the catalytic activities of $Pd/Au/CeO_2$ and the controlled catalysts $Pd/Au/CeO_2$-air and $Pd/Au/CeO_2$-water. The XANES, EXAFS, and HAADF-STEM results revealed that the Pd(II)−(μ-O)−Au(0) structure was formed via the selective oxidation of Pd(0)−Au(0) alloy supported on CeO_2 when the catalyst was exposed to water in an air atmosphere. The dehydrogenation profiles of cyclohexanone to phenol with $Pd/Au/CeO_2$ or Pd−Au/LDH revealed that the dehydrogenation path from 2-cyclohexen-1-one to phenol was different between $Pd/Au/CeO_2$ and Pd−Au/LDH, which indicates that the active site of $Pd/Au/CeO_2$ is not a Pd(0)−Au(0) alloy structure. These results suggest that the Pd(II)−(μ-O)−Au(0) structure is the active site for the efficient α-C−H bond activation of saturated ketones. DFT calculations using the $Pd_1O_2Au_{12}$ cluster model with the Pd(II)−(μ-O)−Au(0) structure revealed the dehydrogenation mechanism of cyclohexanone. The calculation results were consistent with the experimentally determined turnover-limiting step and the activation energy obtained from the Arrhenius plot. Moreover, the calculated activation free energy for 2-cyclohexen-1-one dehydrogenation was significantly greater than that for cyclohexanone dehydrogenation, which was consistent with the selective formation of 2-cyclohexen-1-one using $Pd/Au/CeO_2$. The high regioselectivity of 2-phenylcyclohexanone dehydrogenation was also explained by the cluster model.

In this study, we identified a C−H bond activation mechanism via concerted catalysis in which the Pd(II) species acts as a Lewis acid and the μ-oxo species acts as a Brønsted base simultaneously in the Pd(II)−(μ-O)−Au(0) structure. Such a concept for the efficient catalytic C−H bond activation of liquid-phase organic synthesis by the adjacent Lewis acid−Brønsted base pair of a heterogeneous catalyst is quite rare. The active site structure for target reactions from a mechanistic point of view provides a rational strategy for the development of new molecular transformations using heterogeneous catalysts. Because the heterometallic μ-oxo structures were formed via alloying and reoxidation, it should be possible to tune various adjacent Lewis acid−Brønsted base pair sites easily by choosing different metals. This should make our approach applicable to various catalytic C−H bond activations.

ASSOCIATED CONTENT

Supporting Information

The Supporting Information is available free of charge at https://pubs.acs.org/doi/10.1021/jacsau.1c00433.

Experimental details, additional experimental results, additional DFT calculation results, and Cartesian coordinates of optimized structures (PDF)

AUTHOR INFORMATION

Corresponding Authors

Kazuya Yamaguchi − *Department of Applied Chemistry, School of Engineering, The University of Tokyo, Bunkyo-ku, Tokyo 113-8656, Japan;* orcid.org/0000-0002-7661-4936; Email: kyama@appchem.t.u-tokyo.ac.jp; Fax: +81-3-5841-7220

https://doi.org/10.1021/jacsau.1c00433
JACS Au 2022, 2, 394−406

Takafumi Yatabe − *Department of Applied Chemistry, School of Engineering, The University of Tokyo, Bunkyo-ku, Tokyo 113-8656, Japan;* orcid.org/0000-0001-5504-4762; Email: yatabe@appchem.t.u-tokyo.ac.jp

Authors

Daisuke Takei − *Department of Applied Chemistry, School of Engineering, The University of Tokyo, Bunkyo-ku, Tokyo 113-8656, Japan*

Tomohiro Yabe − *Department of Applied Chemistry, School of Engineering, The University of Tokyo, Bunkyo-ku, Tokyo 113-8656, Japan;* orcid.org/0000-0003-1697-9711

Ray Miyazaki − *Institute for Catalysis, Hokkaido University, Sapporo, Hokkaido 001-0021, Japan;* orcid.org/0000-0001-7210-6646

Jun-ya Hasegawa − *Institute for Catalysis, Hokkaido University, Sapporo, Hokkaido 001-0021, Japan;* orcid.org/0000-0002-9700-3309

Complete contact information is available at: https://pubs.acs.org/10.1021/jacsau.1c00433

Notes

The authors declare no competing financial interest.

■ ACKNOWLEDGMENTS

This work was financially supported by JSPS KAKENHI Grant Nos. 19H02509, 20K22547, and 21K14460. Part of this work was conducted at the Advanced Characterization Nanotechnology Platform of the University of Tokyo, supported by "Nanotechnology Platform" of the Ministry of Education, Culture, Sports, Science and Technology (MEXT), Japan (JPMXP09A21UT0095). We thank Mr. Hiroyuki Oshikawa in Institute of Engineering Innovation for the STEM measurements. We greatly appreciate Dr. Hironori Ofuchi (Japan Synchrotron Radiation Research Institute, SPring-8) for the support of XAFS measurements at BL14B2 (Proposal No. 2021A1620, 2020A1803, 2019B1820, and 2019A1784). Some of the computations were performed using Research Center for Computational Science (RCCS), Okazaki, Japan.

■ REFERENCES

(1) Yeung, C. S.; Dong, V. M. Catalytic Dehydrogenative Cross-Coupling: Forming Carbon-Carbon Bonds by Oxidizing Two Carbon-Hydrogen Bonds. *Chem. Rev.* **2011**, *111*, 1215−1292.

(2) Qin, Y.; Zhu, L.; Luo, S. Organocatalysis in Inert C-H Bond Functionalization. *Chem. Rev.* **2017**, *117*, 9433−9520.

(3) Colby, D. A.; Bergman, R. G.; Ellman, J. A. Rhodium-Catalyzed C-C Bond Formation via Heteroatom-Directed C-H Bond Activation. *Chem. Rev.* **2010**, *110*, 624−655.

(4) Baudoin, O. Transition metal-catalyzed arylation of unactivated C(sp^3)-H bonds. *Chem. Soc. Rev.* **2011**, *40*, 4902−4911.

(5) Ackermann, L. Carboxylate-Assisted Transition-Metal-Catalyzed C-H Bond Functionalizations: Mechanism and Scope. *Chem. Rev.* **2011**, *111*, 1315−1345.

(6) Girard, S. A.; Knauber, T.; Li, C.-J. The Cross-Dehydrogenative Coupling of C_{sp3}-H Bonds: A Versatile Strategy for C-C Bond Formations. *Angew. Chem., Int. Ed.* **2014**, *53*, 74−100.

(7) Hoyano, J. K.; Graham, W. A. G. Oxidative addition of the carbon-hydrogen bonds of neopentane and cyclohexane to a photochemically generated iridium(I) complex. *J. Am. Chem. Soc.* **1982**, *104*, 3723−3725.

(8) Ryabov, A. D. Mechanisms of intramolecular activation of carbon-hydrogen bonds in transition-metal complexes. *Chem. Rev.* **1990**, *90*, 403−424.

(9) Gorelsky, S. I.; Lapointe, D.; Fagnou, K. Analysis of the Concerted Metalation-Deprotonation Mechanism in Palladium-Catalyzed Direct Arylation Across a Broad Range of Aromatic Substrates. *J. Am. Chem. Soc.* **2008**, *130*, 10848−10849.

(10) Walsh, A. P.; Jones, W. D. Mechanistic Insights of a Concerted Metalation-Deprotonation Reaction with $[Cp^*RhCl_2]_2$. *Organometallics* **2015**, *34*, 3400−3407.

(11) Anand, M.; Sunoj, R. B. Palladium(II)-Catalyzed Direct Alkoxylation of Arenes: Evidence for Solvent-Assisted Concerted Metalation Deprotonation. *Org. Lett.* **2011**, *13*, 4802−4805.

(12) Thompson, M. E.; Baxter, S. M.; Bulls, A. R.; Burger, B. J.; Nolan, M. C.; Santarsiero, B. D.; Schaefer, W. P.; Bercaw, J. E. σ Bond metathesis" for C-H bonds of hydrocarbons and Sc-R (R = H, alkyl, aryl) bonds of permethylscandocene derivatives. Evidence for noninvolvement of the π system in electrophilic activation of aromatic and vinylic C-H bonds. *J. Am. Chem. Soc.* **1987**, *109*, 203−219.

(13) Hartwig, J. F.; Bhandari, S.; Rablen, P. R. Addition of Catecholborane to a Ruthenium-Alkyl: Evidence for σ-Bond Metathesis with a Low-Valent, Late Transition Metal. *J. Am. Chem. Soc.* **1994**, *116*, 1839−1844.

(14) Hartwig, J. F.; Cook, K. S.; Hapke, M.; Incarvito, C. D.; Fan, Y.; Webster, C. E.; Hall, M. B. Rhodium Boryl Complexes in the Catalytic, Terminal Functionalization of Alkanes. *J. Am. Chem. Soc.* **2005**, *127*, 2538−2552.

(15) Gao, F.; Goodman, D. W. Pd-Au bimetallic catalysts: understanding alloy effects from planar models and (supported) nanoparticles. *Chem. Soc. Rev.* **2012**, *41*, 8009−8020.

(16) Wang, Y.; Cao, L.; Libretto, N. J.; Li, X.; Li, C.; Wan, Y.; He, C.; Lee, J.; Gregg, J.; Zong, H.; Su, D.; Miller, J. T.; Mueller, T.; Wang, C. Ensemble Effect in Bimetallic Electrocatalysts for CO_2 Reduction. *J. Am. Chem. Soc.* **2019**, *141*, 16635−16642.

(17) Deng, Y.-J.; Tripkovic, V.; Rossmeisl, J.; Arenz, M. Oxygen Reduction Reaction on Pt Overlayers Deposited onto a Gold Film: Ligand, Strain, and Ensemble Effect. *ACS Catal.* **2016**, *6*, 671−676.

(18) Liu, P.; Rodriguez, J. A. Catalysts for Hydrogen Evolution from the [NiFe] Hydrogenase to the $Ni_2P(001)$ Surface: The Importance of Ensemble Effect. *J. Am. Chem. Soc.* **2005**, *127*, 14871−14878.

(19) Miura, H.; Endo, K.; Ogawa, R.; Shishido, T. Supported Palladium-Gold Alloy Catalysts for Efficient and Selective Hydrosilylation under Mild Conditions with Isolated Single Palladium Atoms in Alloy Nanoparticles as the Main Active Site. *ACS Catal.* **2017**, *7*, 1543−1553.

(20) Many C−H bond functionalization reactions have been reported using supported metal nanoparticle catalysts although the reactions involving C−H bond activation are quite rare to date. For a related review, see: Baroliya, P. K.; Chopra, J.; Pal, T.; Maiti, S.; Al-Thabaiti, S. A.; Mokhtar, M.; Maiti, D. Supported Metal Nanoparticles Assisted Catalysis: A Broad Concept in Functionalization of Ubiquitous C-H Bonds. *ChemCatChem.* **2021**, *13*, 4655.

(21) Ghosh, P.; Camellone, M. F.; Fabris, S. Fluxionality of Au Clusters at Ceria Surfaces during CO Oxidation: Relationships among Reactivity, Size, Cohesion, and Surface Defects from DFT Simulations. *J. Phys. Chem. Lett.* **2013**, *4*, 2256−2263.

(22) Ham, H. C.; Stephens, J. A.; Hwang, G. S.; Han, J.; Nam, S. W.; Lim, T. H. Role of Small Pd Ensembles in Boosting CO Oxidation in AuPd Alloys. *J. Phys. Chem. Lett.* **2012**, *3*, 566−570.

(23) Ha, H.; Yoon, S.; An, K.; Kim, H. Y. Catalytic CO Oxidation over Au Nanoparticles Supported on CeO_2 Nanocrystals: Effect of the Au-CeO_2 Interface. *ACS Catal.* **2018**, *8*, 11491−11501.

(24) Liu, J.-C.; Ma, X.-L.; Li, Y.; Wang, Y.-G.; Xiao, H.; Li, J. Heterogeneous Fe_3 single-cluster catalyst for ammonia synthesis via an associative mechanism. *Nat. Commun.* **2018**, *9*, 1610.

(25) Prinz, J.; Pignedoli, C. A.; Stöckl, Q. S.; Armbrüster, M.; Brune, H.; Gröning, O.; Widmer, R.; Passerone, D. Adsorption of Small Hydrocarbons on the Three-Fold PdGa Surfaces: The Road to Selective Hydrogenation. *J. Am. Chem. Soc.* **2014**, *136*, 11792−11798.

(26) Wells, D. H., Jr; Delgass, W. N.; Thomson, K. T. Formation of hydrogen peroxide from H_2 and O_2 over a neutral gold trimer: a DFT study. *J. Catal.* **2004**, *225*, 69−77.

(27) Shang, C.; Liu, Z.-P. Origin and Activity of Gold Nanoparticles as Aerobic Oxidation Catalysts in Aqueous Solution. *J. Am. Chem. Soc.* **2011**, *133*, 9938−9947.
(28) Ato, Y.; Hayashi, A.; Koga, H.; Kawakami, T.; Yamanaka, S.; Okumura, M. Theoretical study of aerobic oxidation of alcohols over Au_{38} nanocluster by a two-step-modeling approach. *Chem. Phys. Lett.* **2019**, *724*, 115−121.
(29) Boronat, M.; Combita, D.; Concepción, P.; Corma, A.; García, H.; Juárez, R.; Laursen, S.; López-Castro, J. D. Making C-C Bonds with Gold: Identification of Selective Gold Sites for Homo- and Cross-Coupling Reactions between Iodobenzene and Alkynes. *J. Phys. Chem. C* **2012**, *116*, 24855−24867.
(30) Zhang, X.; Sun, Z.; Wang, B.; Tang, Y.; Nguyen, L.; Li, Y.; Tao, F. F. C-C Coupling on Single-Atom-Based Heterogeneous Catalyst. *J. Am. Chem. Soc.* **2018**, *140*, 954−962.
(31) Dhital, R. N.; Kamonsatikul, C.; Somsook, E.; Bobuatong, K.; Ehara, M.; Karanjit, S.; Sakurai, H. Low-Temperature Carbon-Chlorine Bond Activation by Bimetallic Gold/Palladium Alloy Nanoclusters: An Application to Ullmann Coupling. *J. Am. Chem. Soc.* **2012**, *134*, 20250−20253.
(32) Boekfa, B.; Pahl, E.; Gaston, N.; Sakurai, H.; Limtrakul, J.; Ehara, M. C-Cl Bond Activation on Au/Pd Bimetallic Nanocatalysts Studied by Density Functional Theory and Genetic Algorithm Calculations. *J. Phys. Chem. C* **2014**, *118*, 22188−22196.
(33) Meeprasert, J.; Namuangruk, S.; Boekfa, B.; Dhital, R. N.; Sakurai, H.; Ehara, M. Mechanism of Ullmann Coupling Reaction of Chloroarene on Au/Pd Alloy Nanocluster: A DFT Study. *Organometallics* **2016**, *35*, 1192−1201.
(34) Miyazaki, M.; Furukawa, S.; Komatsu, T. Regio- and Chemoselective Hydrogenation of Dienes to Monoenes Governed by a Well-Structured Bimetallic Surface. *J. Am. Chem. Soc.* **2017**, *139*, 18231−18239.
(35) Ide, M. S.; Hao, B.; Neurock, M.; Davis, R. J. Mechanistic Insights on the Hydrogenation of α,β-Unsaturated Ketones and Aldehydes to Unsaturated Alcohols over Metal Catalysts. *ACS Catal.* **2012**, *2*, 671−683.
(36) Bobuatong, K.; Sakurai, H.; Ehara, M. Intramolecular Hydroamination by a Primary Amine of an Unactivated Alkene on Gold Nanoclusters: A DFT Study. *ChemCatChem.* **2017**, *9*, 4490−4500.
(37) Zhu, Y.; Cao, T.; Cao, C.; Luo, J.; Chen, W.; Zheng, L.; Dong, J.; Zhang, J.; Han, Y.; Li, Z.; Chen, C.; Peng, Q.; Wang, D.; Li, Y. One-Pot Pyrolysis to N-Doped Graphene with High-Density Pt Single Atomic Sites as Heterogeneous Catalyst for Alkene Hydrosilylation. *ACS Catal.* **2018**, *8*, 10004−10011.
(38) Miyazaki, R.; Jin, X.; Yoshii, D.; Yatabe, T.; Yabe, T.; Mizuo, N.; Yamaguchi, K.; Hasegawa, J. Mechanistic study of C-H bond activation by O_2 on negatively charged Au clusters: α,β-dehydrogenation of 1-methyl-4-piperidone by supported Au catalysts. *Catal. Sci. Technol.* **2021**, *11*, 3333−3346.
(39) Diao, T.; Stahl, S. S. Synthesis of Cyclic Enones via Direct Palladium-Catalyzed Aerobic Dehydrogenation of Ketones. *J. Am. Chem. Soc.* **2011**, *133*, 14566−14569.
(40) Diao, T.; Pun, D.; Stahl, S. S. Aerobic Dehydrogenation of Cyclohexanone to Cyclohexenone Catalyzed by $Pd(DMSO)_2(TFA)_2$: Evidence for Ligand-Controlled Chemoselectivity. *J. Am. Chem. Soc.* **2013**, *135*, 8205−8212.
(41) Tokunaga, M.; Harada, S.; Iwasawa, T.; Obora, Y.; Tsuji, Y. Palladium-catalyzed oxidation of cyclohexanones to conjugated enones using molecular oxygen. *Tetrahedron Lett.* **2007**, *48*, 6860−6862.
(42) Iosub, A. V.; Stahl, S. S. Palladium-Catalyzed Aerobic Dehydrogenation of Cyclic Hydrocarbons for the Synthesis of Substituted Aromatics and Other Unsaturated Products. *ACS Catal.* **2016**, *6*, 8201−8213.
(43) Takei, D.; Yatabe, T.; Jin, X.; Yabe, T.; Mizuno, N.; Yamaguchi, K. CeO_2-Supported Pd(II)-on-Au Nanoparticle Catalyst for Aerobic Selective α,β-Desaturation of Carbonyl Compounds Applicable to Cyclohexanones. *ACS Catal.* **2020**, *10*, 5057−5063.
(44) Frisch, M. J.; Trucks, G. W.; Schlegel, H. B.; Scuseria, G. E.; Robb, M. A.; Cheeseman, J. R.; Scalmani, G.; Barone, V.; Petersson, G. A.; Nakatsuji, H.; Li, X.; Caricato, M.; Marenich, A. V.; Bloino, J.; Janesko, B. G.; Gomperts, R.; Mennucci, B.; Hratchian, H. P.; Ortiz, J. V.; Izmaylov, A. F.; Sonnenberg, J. L.; Williams-Young, D.; Ding, F.; Lipparini, F.; Egidi, F.; Goings, J.; Peng, B.; Petrone, A.; Henderson, T.; Ranasinghe, D.; Zakrzewski, V. G.; Gao, J.; Rega, N.; Zheng, G.; Liang, W.; Hada, M.; Ehara, M.; Toyota, K.; Fukuda, R.; Hasegawa, J.; Ishida, M.; Nakajima, T.; Honda, Y.; Kitao, O.; Nakai, H.; Vreven, T.; Throssell, K.; Montgomery, J. A., Jr.; Peralta, J. E.; Ogliaro, F.; Bearpark, M. J.; Heyd, J. J.; Brothers, E. N.; Kudin, K. N.; Staroverov, V. N.; Keith, T. A.; Kobayashi, R.; Normand, J.; Raghavachari, K.; Rendell, A. P.; Burant, J. C.; Iyengar, S. S.; Tomasi, J.; Cossi, M.; Millam, J. M.; Klene, M.; Adamo, C.; Cammi, R.; Ochterski, J. W.; Martin, R. L.; Morokuma, K.; Farkas, O.; Foresman, J. B.; Fox, D. J. *Gaussian 16*, rev. B.01; Gaussian, Inc.: Wallingford, CT, 2016.
(45) Zhao, Y.; Truhlar, D. G. The M06 suite of density functionals for main group thermochemistry, thermochemical kinetics, noncovalent interactions, excited states, and transition elements: two new functionals and systematic testing of four M06-class functionals and 12 other functionals. *Theor. Chem. Acc.* **2008**, *120*, 215−241.
(46) Andrae, D.; Häußermann, U.; Dolg, M.; Stoll, H.; Preuß, H. Energy-adjusted *ab initio* pseudopotentials for the second and third row transition elements. *Theor. Chim. Acta* **1990**, *77*, 123−141.
(47) Hehre, W. J.; Ditchfield, R.; Pople, J. A. Self—Consistent Molecular Orbital Methods. XII. Further Extensions of Gaussian—Type Basis Sets for Use in Molecular Orbital Studies of Organic Molecules. *J. Chem. Phys.* **1972**, *56*, 2257−2261.
(48) Maestri, G.; Motti, E.; Della Ca', N.; Malacria, M.; Derat, E.; Catellani, M. Of the Ortho Effect in Palladium/Norbornene-Catalyzed Reactions: A Theoretical Investigation. *J. Am. Chem. Soc.* **2011**, *133*, 8574−8585.
(49) Mantina, M.; Valero, R.; Truhlar, D. G. Validation study of the ability of density functionals to predict the planar-to-three-dimensional structural transition in anionic gold clusters. *J. Chem. Phys.* **2009**, *131*, 064706.
(50) Li, B.-W.; Wang, M.-Y.; Liu, J.-Y. DFT study on the mechanism of palladium(II)-catalyzed reaction of allyl-substituted 3,4-dienoate, alkyne and carbon monoxide. *Mol. Catal.* **2020**, *492*, 111028.
(51) Holder, J. C.; Zou, L.; Marziale, A. N.; Liu, P.; Lan, Y.; Gatti, M.; Kikushima, K.; Houk, K. N.; Stoltz, B. M. Mechanism and Enantioselectivity in Palladium-Catalyzed Conjugate Addition of Arylboronic Acids to β-Substituted Cyclic Enones: Insights from Computation and Experiment. *J. Am. Chem. Soc.* **2013**, *135*, 14996−15007.
(52) Taniguchi, K.; Jin, X.; Yamaguchi, K.; Mizuno, N. Supported gold-palladium alloy nanoparticle catalyzed tandem oxidation routes to N-substituted anilines from non-aromatic compounds. *Chem. Commun.* **2015**, *51*, 14969−14972.
(53) Taniguchi, K.; Jin, X.; Yamaguchi, K.; Mizuno, N. Facile access to N-substituted anilines via dehydrogenative aromatization catalysis over supported gold-palladium bimetallic nanoparticles. *Catal. Sci. Technol.* **2016**, *6*, 3929−3937.
(54) Jin, X.; Taniguchi, K.; Yamaguchi, K.; Mizuno, N. Au-Pd alloy nanoparticles supported on layered double hydroxide for heterogeneously catalyzed aerobic oxidative dehydrogenation of cyclohexanols and cyclohexanones to phenols. *Chem. Sci.* **2016**, *7*, 5371−5383.
(55) The Pd K-edge XANES spectrum of Pd-Au/LDH produced by the same method as $Pd/Au/CeO_2$ revealed that the Pd had a valence of almost zero (Figure S2). The Pd K-edge EXAFS spectrum and fittings of Pd−Au/LDH showed a large CN for the Pd−Au bond (Figure S3), which indicates that a Pd(0)−Au(0) alloy structure is mainly present for Pd−Au/LDH.
(56) Yang, G.; Liu, G. New Insights for Self-Assembled Monolayers of Organothiols on Au(111) Revealed by Scanning Tunneling Microscopy. *J. Phys. Chem. B* **2003**, *107*, 8746−8759.
(57) Hinojosa, J. A., Jr; Weaver, J. F. Surface structural evolution during the thermal decomposition of a PdO(101) thin film. *Surf. Sci.* **2011**, *605*, 1797−1806.

https://doi.org/10.1021/jacsau.1c00433
JACS Au 2022, 2, 394−406

(58) Yamazaki, S.; Matsui, T.; Ohashi, T.; Arita, Y. Defect structures in doped CeO_2 studied by using XAFS spectrometry. *Solid State Ion.* **2000**, *136*−*137*, 913−920.
(59) Hinokuma, S.; Fujii, H.; Okamoto, M.; Ikeue, K.; Machida, M. Metallic Pd Nanoparticles Formed by Pd-O-Ce Interaction: A Reason for Sintering-Induced Activation for CO Oxidation. *Chem. Mater.* **2010**, *22*, 6183−6190.
(60) Hiley, C. I.; Fisher, J. M.; Thompsett, D.; Kashtiban, R. J.; Sloan, J.; Walton, R. I. Incorporation of square-planar Pd^{2+} in fluorite CeO_2: hydrothermal preparation, local structure, redox properties and stability. *J. Mater. Chem. A* **2015**, *3*, 13072−13079.
(61) Kumar, S.; Gautam, S.; Song, T. K.; Chae, K. H.; Jang, K. W.; Kim, S. S. Electronic structure study of Co doped CeO_2 nanoparticles using X-ray absorption fine structure spectroscopy. *J. Alloys Compd.* **2014**, *611*, 329−334.
(62) Laulhé, C.; Hippert, F.; Kreisel, J.; Maglione, M.; Simon, A.; Hazemann, J. L.; Nassif, V. EXAFS study of lead-free relaxor ferroelectric $BaTi_{1-x}Zr_xO_3$ at the Zr *K* edge. *Phys. Rev. B* **2006**, *74*, 014106.
(63) Lagarde, P.; Chorro, M.; Roy, D.; Trcera, N. Study by EXAFS of the local structure around Si on silicene deposited on Ag(1 1 0) and Ag(1 1 1) surfaces. *J. Phys.: Condens. Matter* **2016**, *28*, 075002.
(64) Kim, H. Y.; Lee, H. M.; Henkelman, G. CO Oxidation Mechanism on CeO_2-Supported Au Nanoparticles. *J. Am. Chem. Soc.* **2012**, *134*, 1560−1570.
(65) We also constructed a $Pd_1O_2Au_{24}$ structure **4** as the larger cluster model by replacing the Au atom at the vertex with Pd and placing an O atom in the middle of the adjacent Au atom by referring to the Au_{25} structure of Au/CeO_2 reported previously (Figure S13a).[68] When cyclohexanone was brought into close proximity to the cluster, we found a cyclohexanone-adsorbed structure **4-1** (Figure S14). The adsorption state of the substrate can be moved to a more stable state **4-2** where the α-H atom interacts with the O atom of the Pd(II)−(μ-O)−Au(0) structure (Figure S14). The C═O bond distance of cyclohexanone before adsorption was 1.215 Å, which was lengthened to 1.232 Å by adsorption on the Pd atom in **4-2** (Figure S13b). Furthermore, one of the α-H atoms of the adsorbed cyclohexanone molecule was at a distance (3.08 Å) where it interacted with the O atom of the Pd(II)−(μ-O)−Au(0) structure, and its NPA charge (0.291) was larger than that of cyclohexanone substrate (0.278) (Figure S13b). The presence of interaction between the α-H and μ-O, the elongation of the C═O bond of cyclohexanone, and the NBO charge increase of the α-H were the same tendency as the $Pd_1O_2Au_{12}$ cluster model. We then investigated the reaction pathway for the α-C−H bond cleavage of cyclohexanone from the adsorption structure and found a TS structure **4-3** in which the O atom of the Pd(II)−(μ-O)−Au(0) structure acts as a Brønsted base to deprotonate the α-H atom. The activation free energy for the reaction pathway **4-2** → **4-4** (free energy difference between **4-2** and **4-3**) was calculated to be 11.1 kcal/mol (Figure S14), which was in agreement with the case of the $Pd_1O_2Au_{12}$ model (15.4 kcal/mol) and the experimentally determined activation energy (11.3 kcal/mol). Thus, when the cluster size used for the DFT calculations was increased from $Pd_1O_2Au_{12}$ to $Pd_1O_2Au_{24}$, the results of the α-C−H activation step were almost the same as those of the $Pd_1O_2Au_{12}$ model.
(66) A Pd_1Au_{12} structure model (**5**) possessing Pd(0) was also constructed by replacing the Au atom at the vertex with Pd referring to the Au_{13} structure of Au/CeO_2 reported previously.[25] Using the cluster **5**, the α-C−H bond activation pathway of cyclohexanone was investigated. The adsorption of cyclohexanone on Pd or neighboring Au proceeded exothermically in both cases (Figure S15). Through the investigation of the α-C−H bond activation pathways from these adsorbed states, we found the corresponding transition states, respectively. From the structure where cyclohexanone is adsorbed on Au (**5-2**), the α-C−H bond of cyclohexanone was dissociated on Pd with the activation free energy of 29.2 kcal/mol (Figure S15). On the other hand, from the structure where cyclohexanone is adsorbed on Pd (**5-2'**), the α-C−H bond of cyclohexanone was dissociated on both Pd and Au with the activation free energy of 37.7 kcal/mol (Figure S15). These activation free energies of α-C−H bond activation of cyclohexanone were much larger than that using the $Pd_1O_2Au_{12}$ model (15.4 kcal/mol). These DFT calculation results are consistent with the experimental results that the α,β-dehydrogenation of cyclohexanone to 2-cyclohexen-1-one hardly proceeded at 70 °C using the Pd(0)−Au catalysts such as Pd−Au/LDH while the Pd(II)−Au catalysts such as $Pd/Au/CeO_2$ catalyzed the selective α,β-dehydrogenation efficiently, indicating the high importance of the Pd(II)−(μ-O)−Au(0) structure working as a neighboring Lewis acid−Brønsted base pair for the efficient α-C−H activation of cyclohexanone.
(67) Although the present Pd(II)−(μ-O)−Au(0) structure working as a neighboring Lewis acid−Brønsted base pair for the C−H activation is hitherto unknown, there are some reports on catalytic C−H activations promoted by neighboring oxo/hydroxo groups as Brønsted base sites; see: (a) Biswas, S.; Mullick, K.; Chen, S.-Y.; Kriz, D. A.; Shakil, M. D.; Kuo, C.-H.; Angeles-Boza, A. M.; Rossi, A. R.; Suib, S. L. Mesoporous Copper/Manganese Oxide Catalyzed Coupling of Alkynes: Evidence for Synergistic Cooperative Catalysis. *ACS Catal.* **2016**, *6*, 5069−5080. (b) Funes-Ardoiz, I.; Maseras, F. Oxidative Coupling Mechanisms: Current State of Understanding. *ACS Catal.* **2018**, *8*, 1161−1172. (c) Zhang, L.-L.; Li, S.-J.; Zhang, L.; Fang, D.-C. Theoretical studies on CuCl-catalyzed C-H activation/C-O coupling reactions: oxidant and catalyst effects. *Org. Biomol. Chem.* **2016**, *14*, 4426−4435.
(68) Nhat, P. V.; Si, N. T.; Nguyen, M. T. Structural Evolution and Stability Trend of Small-Sized Gold Clusters Au_n (n = 20−30). *J. Phys. Chem. A* **2020**, *124*, 1289−1299.

https://doi.org/10.1021/jacsau.1c00433
JACS Au 2022, 2, 394−406